ELSEVIER

Nuclear Instruments and Methods in Physics Research A 393 (1997) 419–425

NUCLEAR INSTRUMENTS & METHODS IN PHYSICS RESEARCH Section A

Visualization and simulation of electron beam transport along a FEL planar wiggler

A. Abramovich*, M. Arbel, L. Gilutin, H. Kleinman, A. Eichenbaum, I.M. Yakover, Y. Pinhasi, I. Marhasine A. Gover

Faculty of Engineering – Physical Electronics, Tel-Aviv University, Ramat Aviv 69978, Israel

Abstract

We have developed and employed a special apparatus for viewing and investigating the motion and behavior of an e-beam inside a planar wiggler. The total current $I(z)$, the current density $J(x, y, z)$, the beam position and cross-section shape were investigated along an evacuated waveguide cavity located on the axis of the wiggler of the TAU 70 KeV FEM. The beam cross-section image could be viewed on the screen through a window at the end of the evacuated waveguide using a CCD camera equipped with a zoom lens.

An exact 3D simulation code (PTIMF) developed in our group for simulation of electron trajectories inside and along the wiggler, was used to calculate trajectories of electrons in the wiggler region under conditions similar to those prevailing in the experiment. The correlation of experimental results with those predicted from simulations was good. It is presented and discussed in this paper.

1. Introduction

Detailed knowledge of the e-beam parameters during transport through a wiggler of a Free-Electron Laser (FEL) or other electron devices is important in order to enable improvement and prediction of the device performance. These parameters (beam current, beam dimension and beam position) are used as input data for simulation codes FEL3D and MALT1D which are used by us to predict FEL performance [1–3]. Undesired electron trajectories inside a planar wiggler may limit the gain and output power expected for a given set of FEL parameters. There are several factors which influence the electron trajectory in the electron beam such as wiggler magnetic field characteristics, e-beam initial conditions and focusing [4–6]. A planar wiggler has a natural focusing in the vertical (y) direction, normally the direction of the magnetic field, but no focusing in the lateral (x) direction, so that the beam may disperse in that direction if no additional focusing means are provided. The planar wiggler used in the Tel-Aviv University (TAU) FEM [7,8], has a novel lateral focusing scheme. A pair of longitudinal permanent SmCo magnets each located on either side of the wiggler [6] is used. We also added three matching magnets at the entrance and exit of the wiggler in order to suppress off-axis drift and to control the angle of electron trajectories [6]. Fig. 1 shows a schematic of the novel planar wiggler used in the mini FEM at (TAU) and Table 1 summarizes its parameters.

2. Experimental set-up

A special apparatus for viewing and investigating the e-beam inside the planar wiggler was developed and employed by us (see Fig. 2). This apparatus consists of a movable quartz fluorescent screen on which the beam cross section and beam center position along the entire wiggler length can be viewed and recorded by use of a CCD camera with a telescopic zoom lens. We measured the total current of the e-beam from the current collected by a metal mesh covering the quartz screen and correcting the measurement by an appropriate factor due to electron scattering and secondary emission. For our 70 KeV e-beam, the total beam current is about 40% higher than the current measured on the screen [9–11]. The beam viewing apparatus was installed in a rectangular evacuated waveguide located on the axis of the planar wiggler of our FEM. A CCD camera placed in front of a window at one end of the waveguide enabled recording

* Corresponding author. Fax: +972 36423 508.

PII S0168-9002(97)00537-8

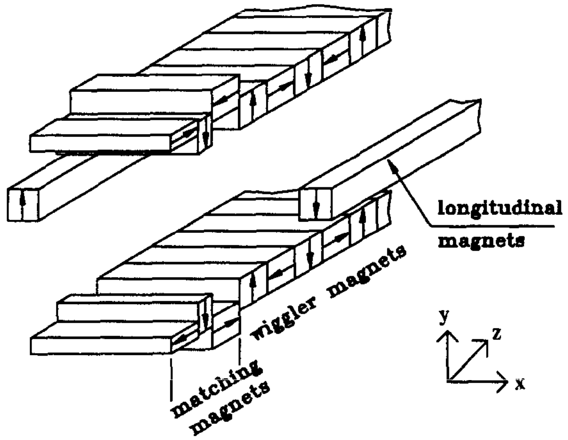

Fig. 1. Scheme of TAU FEM planar wiggler with two longitudinal permanent magnets for horizontal focusing and sets of matching magnets at both ends of the wiggler for optimization of beam entrance and exit.

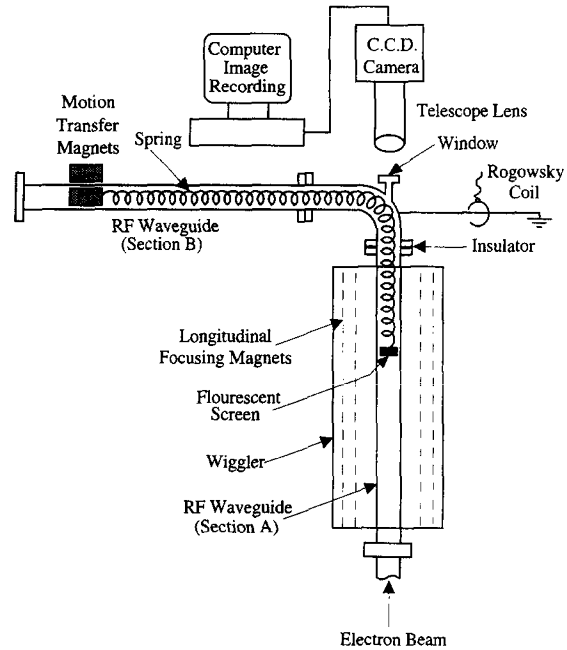

Fig. 2. Schematic of the beam viewing apparatus.

Table 1
Planar wiggler parameters

E-beam energy	70 KeV
Wiggler field	$B_w = 300$ G
Wiggler parameter	$a_w = 0.12$
Period length	$\lambda_w = 4.44$ cm
Number of periods	$N_w = 17$
Calculated betatron wave number	$k_{\beta x} = k_{\beta y} = 23.4$ rad/m
Calculated betatron wavelength	$\lambda_{\beta x} = \lambda_{\beta y} = 0.268$ m
Calculated wiggling amplitude	$x_w = 1.76$ mm
Waveguide dimension	22.15×47.55 mm
E-beam current	$I_b = 600$ mA

of the beam shape and position; the data were stored in the computer memory for further processing. The screen was moved along the waveguide by magnetic coupling through the vacuum envelope to a rigid spring attached to the fluorescent screen.

3. Wiggler operation and simulation

The power and efficiency attained in a FEL depend significantly on the quality of e-beam transport through the wiggler. Maximum power is extracted from the e-beam if the average position of the electron trajectories is along the waveguide and wiggler axis, where the electric field is maximal. In addition, the use of a depressed collector for efficiency enhancement is based on transport of the e-beam to a collector which is located after the wiggler exit. A nearly 100% transport through the wiggler region is essential for efficient depressed collector operation [12,13].

The electron trajectory of electrons in the e-beam is governed by the applied fields and by the e-beam space-charge forces. For a single-particle model, the particle trajectory is described by the Lorentz equation:

$$\gamma m \frac{\mathrm{d}\boldsymbol{v}}{\mathrm{d}t} = -e\boldsymbol{v} \times \boldsymbol{B}, \tag{1}$$

where γ is the relativistic factor, m is the particle mass, $\boldsymbol{v}$ is the velocity of the particle, e is the particle charge and $\boldsymbol{B}$ is the magnetic field. The magnetic field of the wiggler and the two lateral focusing long magnets (see Fig. 1) is given by [6]

$$\boldsymbol{B}_w = B_w(\hat{\boldsymbol{e}}_y \cosh k_w y \cos k_w z - \hat{\boldsymbol{e}}_z \cosh k_w y \cos k_w z) - \alpha_R x \hat{\boldsymbol{e}}_y, \tag{2}$$

where $\boldsymbol{B}_w$ is the wiggler magnetic field, B_w is the amplitude of the wiggler magnetic field, k_w is the wiggler wave number $(2\pi/\lambda_w)$ and α_R is the lateral magnetic gradient of the focusing magnets. If one solves the Lorentz equation (Eq. (1)) using the magnetic field distribution (Eq. (2)), one finds that the particle trajectory exhibits

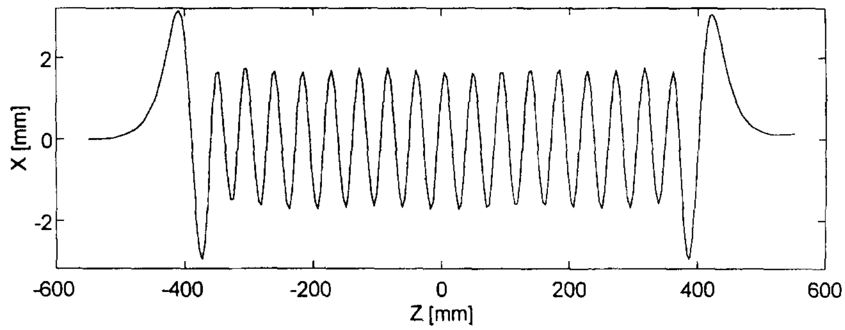

Fig. 3. PTIMF simulation code results for a particle trajectory (X-direction) inside a planar wiggler with initial conditions $x = 0$, $y = 0$, $v_x = 0$, and $v_y = 0$.

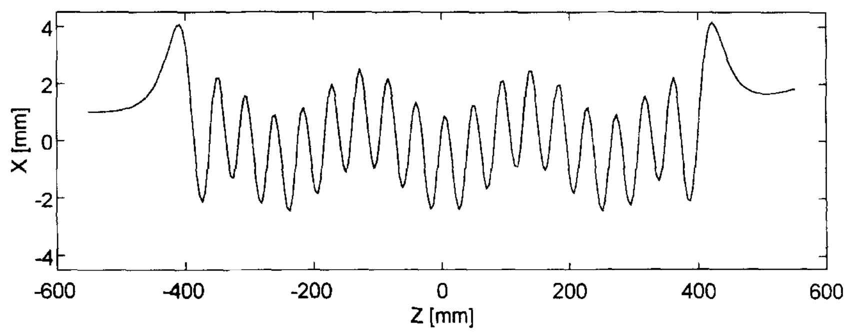

Fig. 4. PTIMF simulation code results for a particle trajectory (X-direction) inside a planar wiggler with initial condition $x = 1$ mm, $y = 0$, $v_x = 0$, and $v_y = 0$.

betatron oscillations in the X- and Y-directions [6]:

$$k_{\beta x} = \sqrt{\frac{e\alpha_R}{\gamma m v_{0z}}}, \tag{3}$$

$$k_{\beta y} = \frac{k_\beta}{\sqrt{1 - \left(\frac{k_{\beta x}}{k_\beta}\right)^2}}, \tag{4}$$

where $k_{\beta x}$ and $k_{\beta y}$ are the horizontal and vertical betatron wave numbers respectively, v_{oz} is the mean axial velocity of the particle and k_β is the conventional planar wiggler betatron wave number (without focusing magnets) given by

$$k_\beta = \frac{a_w k_w}{\sqrt{2}\gamma \beta_{0z}}, \tag{5}$$

where $a_w = eB_w/(k_w mc)$ is the wiggler parameter and $\beta_{0z} = v_{0z}/c$ (c is speed of light). If the initial conditions of the particle at the wiggler entrance are $x = 0$, $y = 0$, $v_x = 0$ and $v_y = 0$, no betatron oscillations occur and the particle performs ideal wiggling in the X-direction about the axis (see Fig. 3). The amplitude x_w of the wiggling motion is

$$x_w = \frac{\sqrt{2}k_\beta}{k_w^2}. \tag{6}$$

If the initial velocities and position of the particle differ from zero, a betatron oscillation occurs in addition to the wiggling motion (see Figs. 4–6). The betatron oscillation amplitude is determined by the wiggler parameters and the initial condition of the particle at the wiggler entrance [6]. The larger the initial velocities and the position offset from zero the greater is the betatron oscillation amplitude (see Fig. 6).

A new 3D simulation code Particle Transport In Magnetic Field (PTIMF) was developed by the FEL group at TAU in order to investigate particle trajectories inside of our special planar wiggler. We used the PTIMF code also to determine the value of the required gaps between the matching magnets at the entrance end and at the exit end of the wiggler. The PTIMF simulation code is based on an exact 3D magnetic field calculation using the four facets to describe each magnet bar [14].

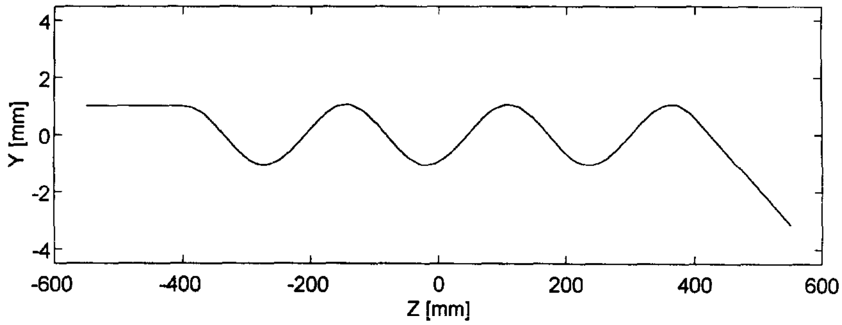

Fig. 5. PTIMF simulation code results for a particle trajectory (Y-direction) inside a planar wiggler with initial condition $x = 0$, $y = 1$ mm, $v_x = 0$ and $v_y = 0$.

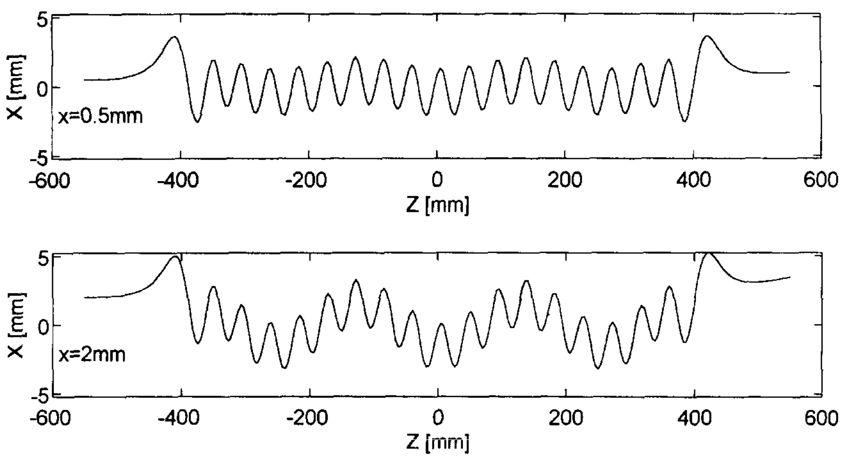

Fig. 6. Betatron amplitude for two different cases: $x = 0.5$ mm, $x = 2.0$ mm.

Figs. 3–6 show the trajectories of a particle inside the wiggler for various initial conditions.

4. Experimental results

We measured experimentally the e-beam position, current and e-beam cross section along the waveguide located inside the planar wiggler (see Fig. 2). These parameters of the e-beam serve also as input data for FEL performance simulation codes. We found experimentally that the wiggler averaged e-beam trajectory departs from the axis, and that the e-beam current decreases as we advance along the axis. The imperfection of e-beam transport through the wiggler is related to inaccuracies in the wiggler construction, nonuniformity of the magnets and alignment problems. We improved the e-beam trajectory by adding external correction magnets to the wiggler (to correct for average e-beam deviations from the axis). These correction magnets were placed at various positions along the wiggler so that the average e-beam trajectory is closer to the axis along the entire planar wiggler. Fig. 7 shows the e-beam center location (in the X- and Y-direction) along the axis (Z-direction) of the planar wiggler after placement of the external correction magnets.

The cross-sectional size of the e-beam increases as the beam advances along the planar wiggler (from an initial diameter of 3 to 5 mm at the wiggler exit). Fig. 8 shows the e-beam cross section as recorded by a CCD camera near the wiggler entrance (Fig. 8, left) and near the wiggler exit (Fig. 8, right). The marks above the e-beam image shown in Fig. 8, left, are due to the cathode light scattered from the e-gun. Fig. 9 shows the e-beam radius along the wiggler. It can be seen that the e-beam radius increases and decreases periodically along the wiggler (scalloping effect).

Another goal of the experiment was to measure and view the wiggling motion of the e-beam along the planar wiggler. In order to view the wiggling motion, we

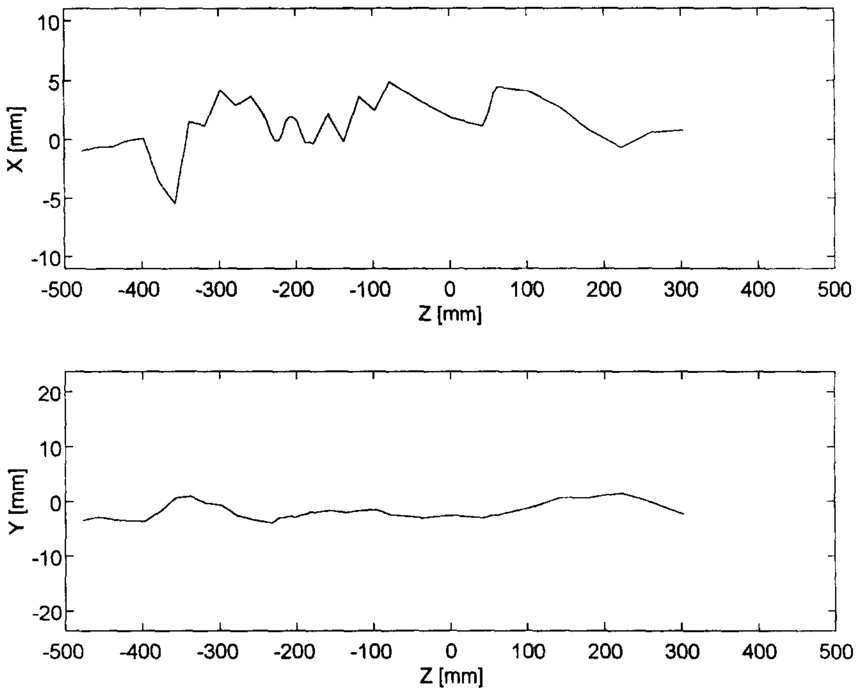

Fig. 7. E-beam average trajectory inside of TAU planar wiggler with external correction magnets (X-direction top, Y-direction bottom).

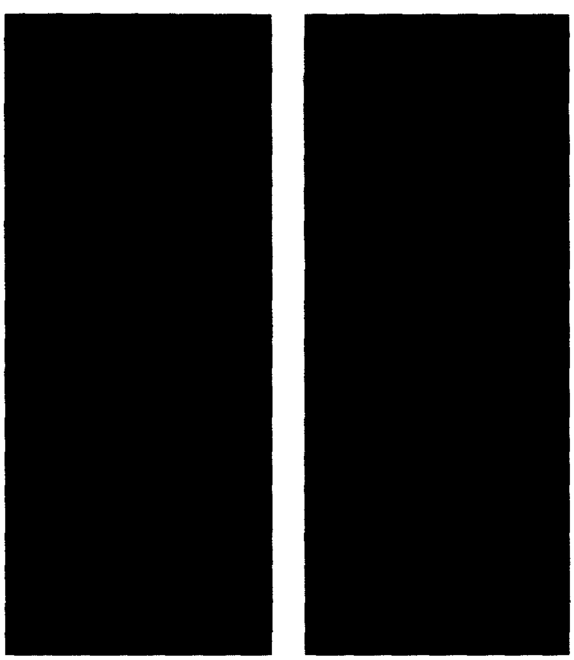

Fig. 8. E-beam cross-section at the entrance (left) and exit (right) of the wiggler.

recorded (by use of a CCD camera) about 60 images of the e-beam obtained at different positions along the axis with steps of 2 mm from each other. We stored these images in the computer for further processing. Fig. 10 shows the trajectory of the e-beam center in two sections of the planar wiggler where we did not use external correction magnets. The circles in Fig. 10 indicate measured points and the solid line indicates the computed best fit to the measured points. We also processed and recorded the e-beam cross-section dimensions and the beam spot nutation angle. Fig. 11 illustrates the e-beam cross-section development and beam spot nutation effects in the second measured section between $z = +120$ mm and $z = +230$ mm.

5. Comparison of theoretical and experimental results and discussion

The analytically calculated beam wiggling amplitude $x_w = 1.76$ mm (given in Table 1) is in excellent agreement with the PTIMF simulation code results given in Figs. 3–6. The measured value of the wiggling amplitude obtained from sinusoidal curve fitting to the measured data (see Fig. 10) is $x_w \sim 1.65$ mm. (This is also in good agreement with an analytical calculation and simulation results.) The difference is, in part, due to difficulties in

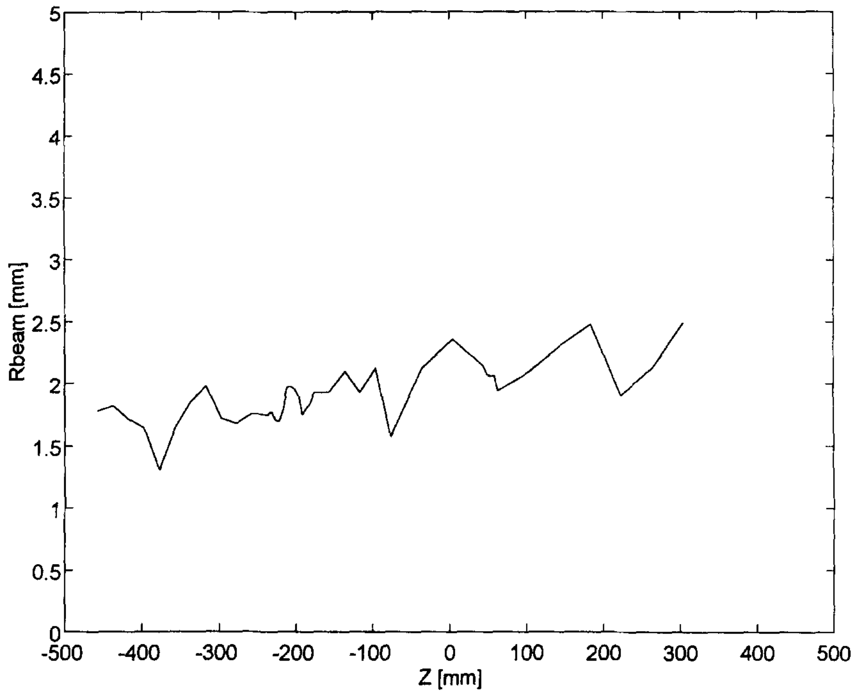

Fig. 9. E-beam radius variation (scalloping) along the wiggler.

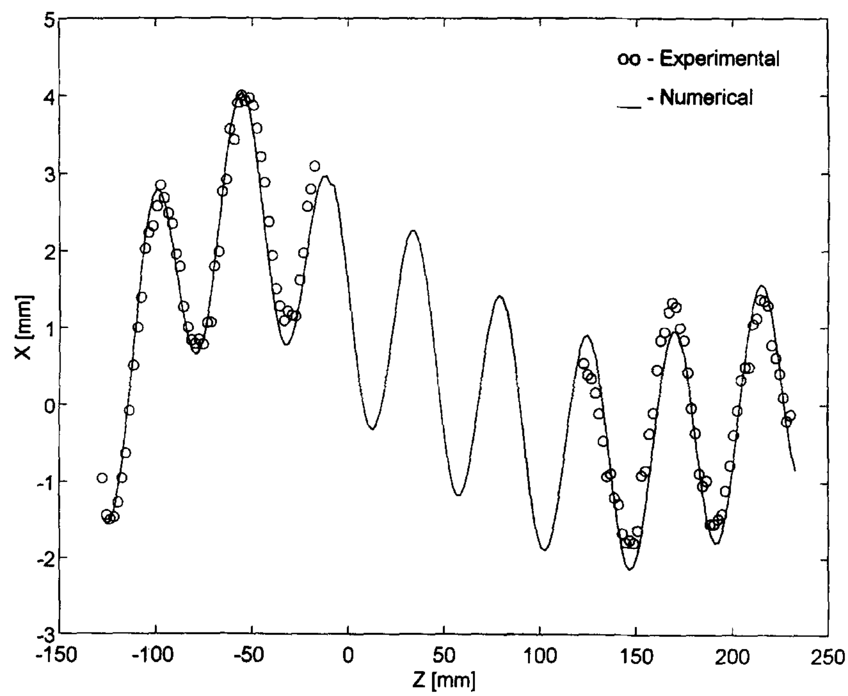

Fig. 10. Wiggling of the e-beam inside the wiggler (circles indicate measured points and the solid line is computed best fit to the e-beam trajectory).

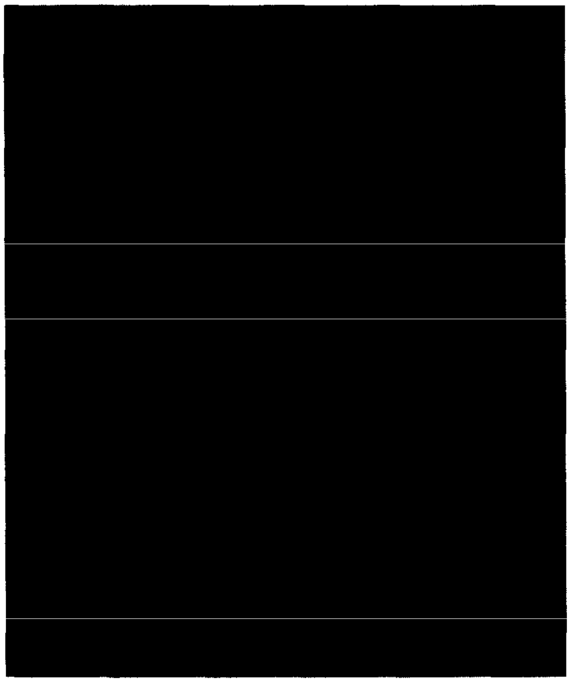

Fig. 11. E-beam cross-section CCD camera recordings along a section of the wiggler.

determining the e-beam center position. The period of the beam envelope scalloping shown in Fig. 9 is related to betatron oscillation period by a factor of two ($\lambda_\beta = 2\lambda_{\text{scalloping}}$) [15]. From this relation the betatron oscillation period is found to be 270 mm which is in excellent agreement with the calculated value given in Table 1. We also observed in Fig. 11 a nutation of the e-beam cross section. In one scalloping period also the main diameter of the ellipsoidal beam cross section changes orientation from a left inclination to a right inclination and back. This may be related to different focusing forces in the X and Y dimension ($k_{\beta x} \neq k_{\beta xy}$) and nonsymmetrical initial conditions.

In this work we found experimentally all the important parameters of e-beam transport trough planar wigglers such as wiggling amplitude, wiggling period, position, shape and rotation of the e-beam, scalloping and betatron oscillation. Also, the experiment enabled improvement and correction of the e-beam transport along the wiggler as well as attainment of input parameters for FEL simulation codes. The comparison of the experimental results and e-beam transport simulations codes show excellent agreement.

References

[1] Y. Pinhasi, M. Cohen, A. Gover, Int. J. Electron. 78 (1995) 581.

[2] A. Abramovich et al., Nucl. Instr. and Meth. A 375 (1996) 164

[3] M. Caplan et al., Nucl. Instr. and Meth. A 358 (1995) 174.

[4] E.T. Scharlemann, J. Appl. Phys. 58 (1985) 2154.

[5] P. Diament, Phys. Rev. A 23 (1981) 2537.

[6] M. Cohen, Ph.D. Dissertation, Tel-Aviv University, Issrel, 1996.

[7] M. Cohen, et al., Nucl. Instr. and Meth. A 358 (1993) 82.

[8] M. Cohen et al., Phys. Rev. Lett. 74 (1995) 3812.

[9] M. Arbel, M.Sc. Theses, Tel-Aviv University, Issral, 1995.

[10] J.I. Goldstein et al., Scanning Electron Microscopy and X-ray Microanalysis, Plenum press, 1994.

[11] D.C. Joy, J. Microscopy 147(1) (1987) 164.

[12] H.G. Kosmahl, Proc. IEEE 70 (1982) 1325.

[13] A. Eichenbaum et al., these Proceedings (18th Free Electron Laser Conf., Rome, Italy, 1996) Nucl. Instr. and Meth. A 393 (1997) 361.

[14] L. Elias et al., properties of the UCSB FEL wiggler, Proc. SPIE vol. 453 (1983) pp. 160–171.

[15] A. Gover et al., in: K. Button (Ed.), Design Consideration for Free Electron Lasers, Academic Press, 1984.